

# Chapter 6

## Growth and doping of ZnO nanobelts

### 6.1. Introduction

A minor variation of growth conditions in thermal evaporation method especially the substrates and source temperatures may result in great change of morphologies of final products. The belt-like nanostructure morphology is a common structural characteristic for functional oxides with different crystallographic structures. Such morphology could be obtained in the high temperature of the source material in thermal evaporation method. Also, the native structural properties of materials are another important factor for the formation of those one dimensional nanostructures. In addition, one of the best ways to improve and modify of nanostructures properties with belt shape is doping of nanobelts with selective elements.

In this chapter, the optical behaviors of ZnO nanobelts are presented, which are doped with S and Sn as two different types of doping materials by photoluminescence spectroscopy. In addition, the effect of annealing at 600 °C on the PL results of these nanobelts is studied. The S-doped ZnO nanobelts show a significant effect in the visible region while the Sn-doped ZnO nanobelts exhibit greater effect in the UV region. Furthermore, the effects of the annealing temperature at 400 and 600 °C on the structural and optical properties of the S-doped ZnO nanobelts are investigated.

### 6.2. S- and Sn-doped ZnO nanobelts

#### 6.2.1. Experimental details

The nanobelts were deposited in a conventional horizontal furnace on Si(111) substrates. ZnO (99.99%)/SnO<sub>2</sub> (99.99%) (Mol 10:2) and ZnO/MgSO<sub>4</sub>·7H<sub>2</sub>O (Mol

10:2) powders were used as the source materials for growth of the Sn- and S-doped ZnO nanobelts, respectively. The ZnO/SnO<sub>2</sub> powder was placed on an alumina boat and inserted into a horizontal tube furnace, in order to serve as the evaporation source. Silicon clean process is similar to previous chapters. The source material was heated up to 1200 °C, and the temperature of the substrate was maintained at 800 °C during the growth process of the Sn-doped ZnO nanobelts. All conditions for growth of the S-doped ZnO nanobelts were the same as those for the Sn-doped ZnO nanobelts except for the position of MgSO<sub>4</sub>.7H<sub>2</sub>O and the substrate in the furnace. MgSO<sub>4</sub>.7H<sub>2</sub>O and the Si substrate were placed at 850 and 700 °C respectively, downstream of the source material (ZnO powder) during the growth process of the S-doped ZnO nanobelts. We used ZnO with SnO<sub>2</sub> at the same temperature in the furnace, due to their similar melting points, but the melting point of ZnO and MgSO<sub>4</sub>.7H<sub>2</sub>O are very different, so they were placed at different locations in the furnace. We have also grown the undoped ZnO nanobelts with the same conditions that have applied for growth of the Sn-doped ZnO nanobelts. High-purity N<sub>2</sub> gas was fed at about 100 sccm into the tube furnace at one end, while the other end was connected to a rotary pump. The growth process was allowed to proceed for 1 h. A vacuum of 800 Pa was maintained inside the tube furnace during the deposition of the nanostructures.

### **6.2.2. Results and discussion**

Figures 6.1 (a<sub>1</sub>-b<sub>1</sub>) show FESEM images of the S- and Sn-doped ZnO nanobelts, respectively. The typical average widths of the S- and Sn-doped ZnO nanobelts were about 73 and 121 nm respectively, with a thickness of a few nanometers and a length of several micrometers. This difference in the size of the nanobelts could be attributed to the different processing temperatures of the samples (supersaturation). Figures 6.1 (a<sub>2</sub>-

b<sub>2</sub>) show high-magnification images of individual S- and Sn-doped ZnO nanobelts, respectively.

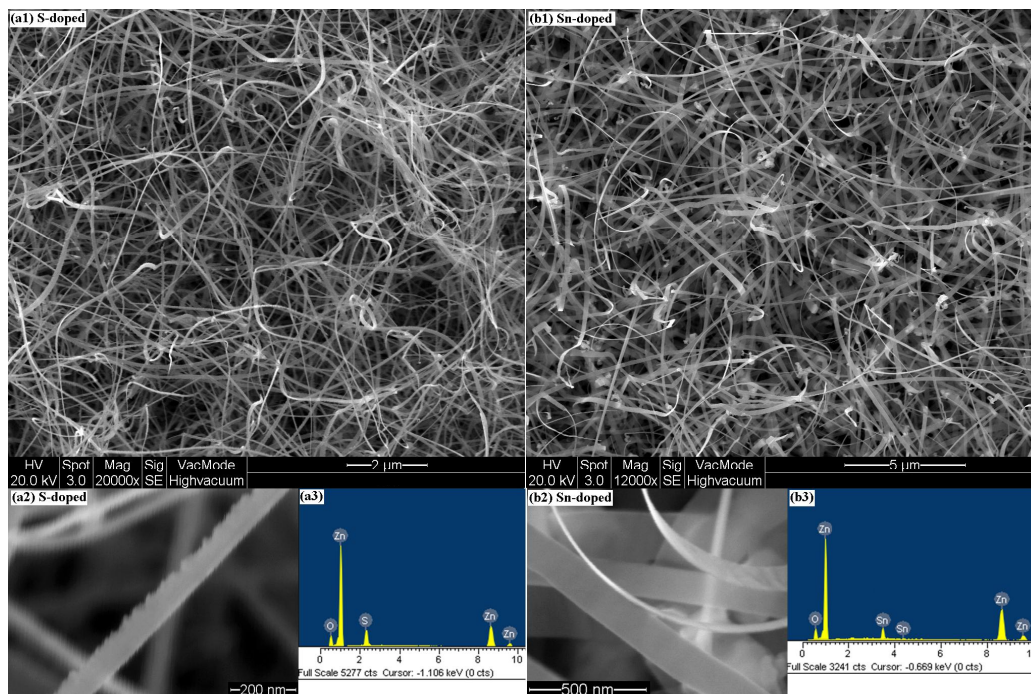
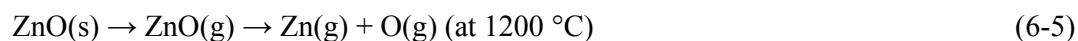
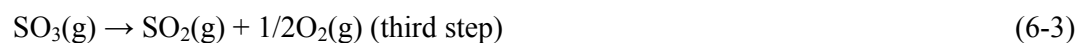
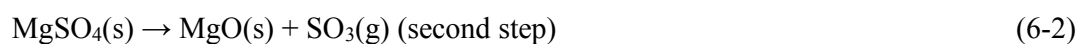
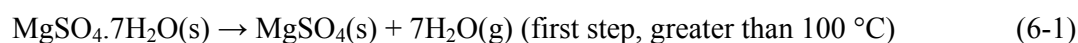


**Figure 6.1.** (a<sub>1</sub>, b<sub>1</sub>) FESEM images of the S- and Sn-doped ZnO nanobelts, respectively. (a<sub>2</sub>, b<sub>2</sub>) High-magnification FESEM image of a single S- and Sn-doped ZnO nanobelt, respectively. (a<sub>3</sub>, b<sub>3</sub>) EDX spectra of a single S- and Sn-doped ZnO nanobelt.

Figure 6.1 (a<sub>2</sub>) shows that the S-doped ZnO nanobelt is not smooth on one of its sides, while Fig. 6.1 (b<sub>2</sub>) shows that the Sn-doped ZnO nanobelt is smooth on both sides. This difference could be the first difference between an anionic and cationic doping material in ZnO nanobelts that can be attributed to the different O and Zn treatment in the ZnO structure. Of course, further studies are needed to fully explain this difference. The EDX spectra of the two samples are shown in Figs. 6.1 (a<sub>3</sub>-b<sub>3</sub>). The S and Sn contents are about 12% and 8% (atomic), respectively. It can be seen that, the content of S in the S-doped ZnO nanobelts is greater than the content of Sn in the Sn-doped ZnO nanobelts, which may be due to the lower melting point of MgSO<sub>4</sub> in comparison to SnO<sub>2</sub>. No Mg peak is detected in the EDX spectrum of the S-doped ZnO nanobelts.

The use of a ZnO/SnO<sub>2</sub> mixture as a source material for Sn-doping in ZnO nanostructures is very common, but the use of MgSO<sub>4</sub>.7H<sub>2</sub>O as a source for S-doping in ZnO may be a new method for producing S-doped ZnO nanostructures. FeS ( Hussain *et al.*, 2007a; Hussain *et al.*, 2007b; Shen *et al.*, 2005a) and ZnS (Foreman *et al.*, 2006; Geng *et al.*, 2003) are two common materials for doping sulfur in ZnO nanostructures by the vapor deposition method. Based on this, it is explained the S-doping process here by MgSO<sub>4</sub>.7H<sub>2</sub>O. Certainly, 7H<sub>2</sub>O will evaporate as the furnace temperature increases. Therefore, the process of the S-doping in ZnO nanobelts may be described by the following reactions:



According to the EDX spectrum (Fig. 6.1 (a<sub>3</sub>)), Mg was not found in the synthesized products due to the high melting point of MgO. The EDX result of the remaining materials in the boat also showed that the majority of this material after deposition was MgO.

Figure 6.2 shows FESEM image and EDX spectrum of the undoped ZnO nanobelts that have grown with the same conditions of the Sn-doped ZnO nanobelts. The EDX shows that the nanobelts are undoped ZnO. The sizes of these nanobelts are similar the Sn-doped ZnO nanobelts sizes. In fact, this result shows that impurities do

not any effect on the nanobelts sizes and substrate position in the furnace is the most important factor for the nanobelts sizes.

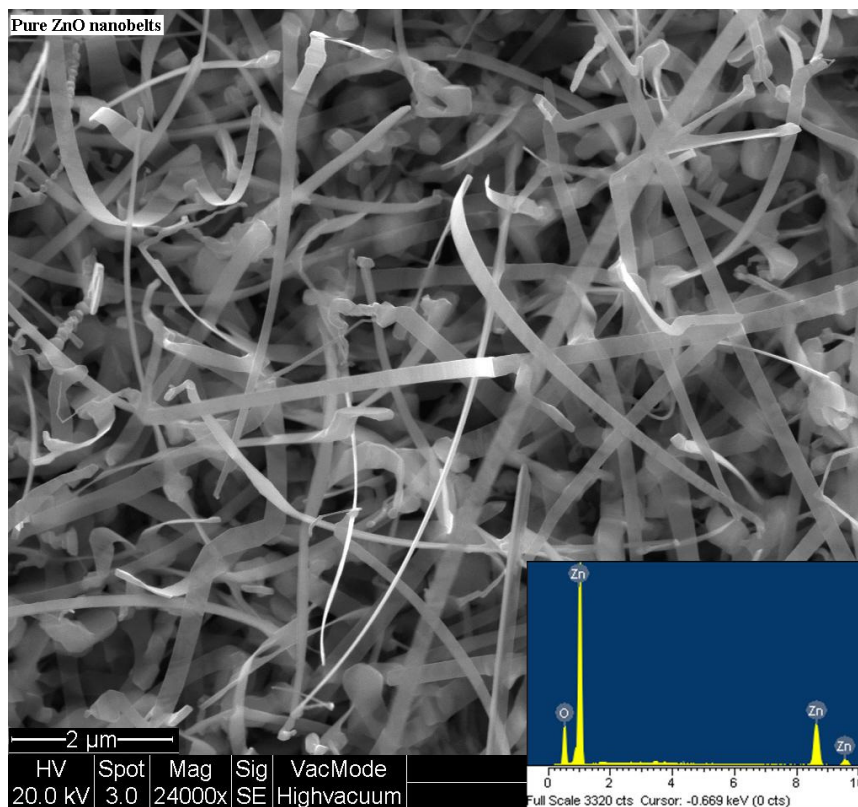


**Figure 6.2.** FESEM image and EDX spectrum of the undoped ZnO nanobelts.

Figure 6.3 shows the XRD patterns of the S-doped, Sn-doped, and undoped ZnO nanobelts. The XRD patterns in Fig. 6.3 agree with the standard card of bulk ZnO with a hexagonal structure, and no diffraction peaks from other impurities were detected. All XRD patterns in Fig. 6.3 show that the preferred orientation of the ZnO nanobelts is (101). It is known that the ionic radius of the substitute  $S^{2-}$  (0.18 nm) is larger than that of  $O^{2-}$  (0.14 nm). Thus, doping with S causes a slight shift of about  $0.18^\circ$  for the (101) XRD peak toward the lower diffraction angle. On the other hand, the (101) peak of the Sn-doped ZnO nanobelts has a slight shift of about  $0.1^\circ$  toward the larger diffraction angle due to the smaller ionic radius of Sn (0.069 nm) as compared to Zn (0.074 nm). These shifts are shown in the inset of Fig 6.3. The FWHM values of all of the peaks of the S-doped ZnO nanobelts are larger than those of the Sn-doped and undoped ZnO

nanobelts. These bigger FWHM values of XRD peaks of the S-doped sample in comparison to the Sn-doped ZnO nanobelts could be due to the larger relative difference in the radii of S and O (22%), as compared to Sn and Zn (6%).

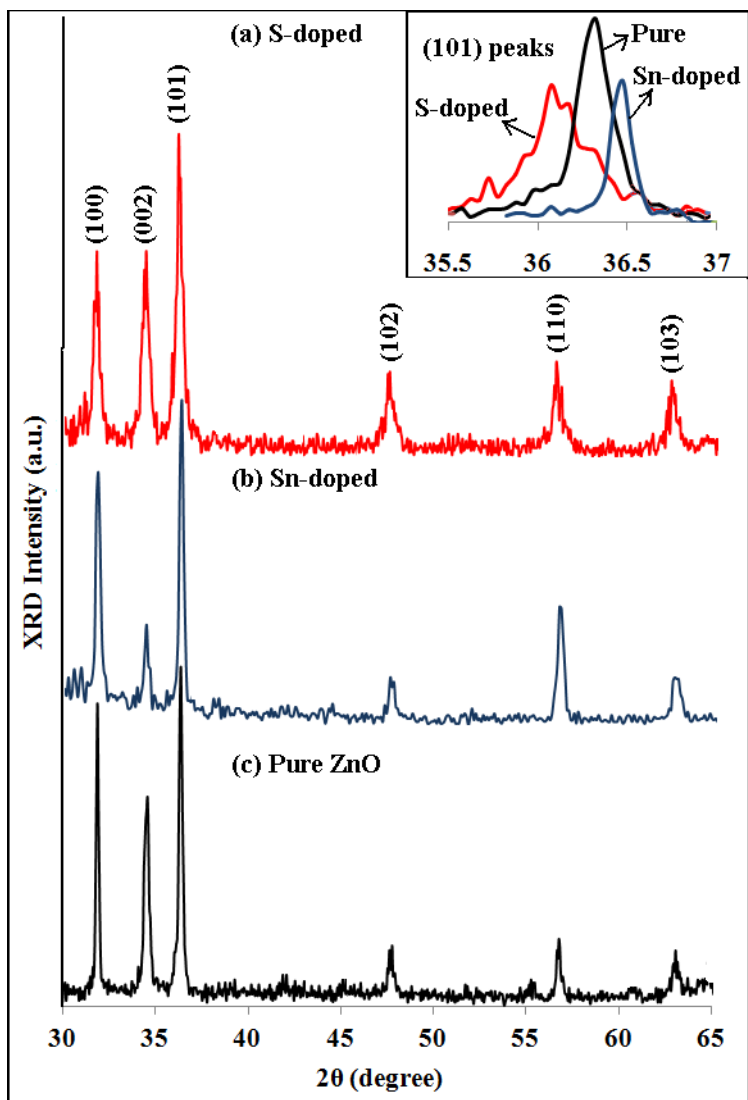


**Figure 6.3.** XRD patterns of the S-doped, Sn-doped, and undoped ZnO nanobelts. All patterns agree with the standard card of bulk ZnO with a hexagonal structure, and no peaks from other impurities are detected. The inset shows the shifts of (101) peaks of the S- and Sn-doped ZnO nanobelts in comparison to the (101) peak of the undoped ZnO nanobelts.

Growth of S-doped ZnO nanobelts in lower temperature zone than Sn-doped and undoped ZnO nanobelts could be also another reason for bigger FWHM. It is known, crystalline quality of nanostructures improves when they grow in higher temperature

(Umar & Hahn, 2008). In addition, the high resolution of (101) peaks shows the uniform peaks for the undoped and Sn-doped ZnO nanobelts (as shown in the inset Fig. 6.3).

Figure 6.4 shows the room temperature PL spectra of the S-doped, Sn-doped, and undoped ZnO nanobelts. It can be seen that there is a significant difference between the PL spectrum of the S-doped nanobelts and other nanobelts. The PL spectra of the Sn-doped and undoped ZnO nanobelts indicate the UV peaks at 376 and 380 nm as well as the green emission peaks at 508 and 513 nm, respectively. Stronger UV peak of the undoped ZnO than the Sn-doped ZnO nanobelts and similar green emission peaks intensity indicate the higher crystalline quality of the undoped ZnO nanobelts than the Sn-doped ZnO nanobelts. In addition, the UV peak of the Sn-doped ZnO nanobelts is blue-shifted by about 4 nm, as compared to the undoped ZnO nanobelts (as shown in the inset in Fig. 6.4 (a)). This blue-shift comes from the modulation of the band-gap that is caused by SnO<sub>2</sub> (Shi *et al.*, 2007). The PL spectrum of the S-doped ZnO nanobelts shows no detectable UV peak and the visible emission peaks in the blue (480 nm) and green (505 and 518 nm) emissions regions. Similar such peaks have observed in other reports of S-doped ZnO nanostructures ( Hussain *et al.*, 2007a; Hussain *et al.*, 2007b; Shen *et al.*, 2005b). In fact, Fig. 6.4 (a) shows that the S-doped ZnO nanobelts have very high concentrations of oxygen vacancies. Since sulfur has a larger ionic radius than oxygen, the incorporation of S into the ZnO lattice will introduce lattice distortion. This effect influences the energy band structure of the ZnO nanobelts doped with sulfur, and as a result, new defects such as oxygen vacancies can be introduced by the new band structure deformation. Based on this reason, the green emission or DLE peak is the strongest peak in the PL result of the S-doped ZnO nanobelts. Moreover, the DLE peak in the S-doped ZnO nanobelts shows a blue-shift in comparison to the DLE peak in the

Sn-doped and undoped ZnO nanobelts. This blue-shift could be attributed to a change in oxygen vacancy centers caused by the substitute O with S.

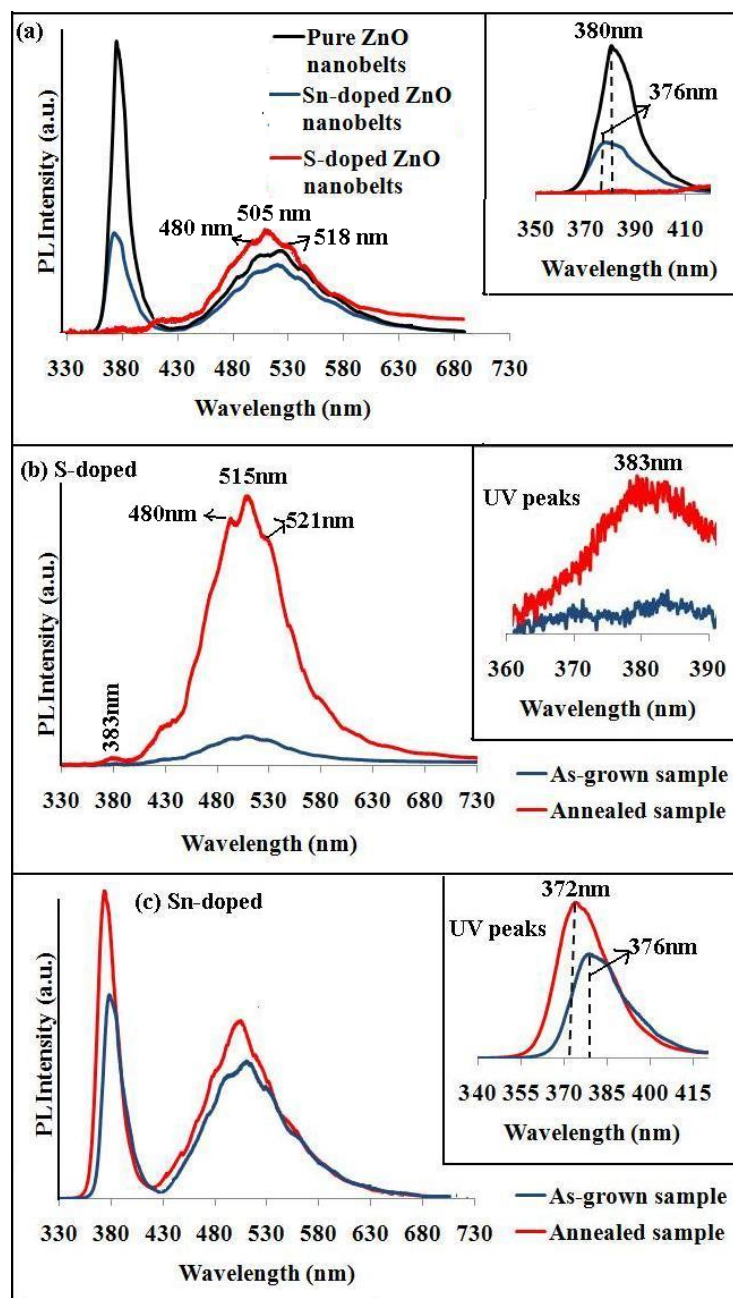


**Figure 6.4.** (a) PL spectra of the S-doped, Sn-doped, and undoped ZnO nanobelts. The inset shows that the UV peak of Sn-doped ZnO nanobelts is blue-shifted in comparison to the undoped ZnO nanobelts. (b) PL spectra of the S-doped ZnO nanobelts, as-grown and annealed at 600 °C for 1h. The inset shows the appearance of a UV peak at 383 nm after annealing. (c) PL spectra of the Sn-doped ZnO nanobelts, as-grown and annealed at 600 °C for 1h. The inset exhibits a blue-shift for the UV peak after annealing.

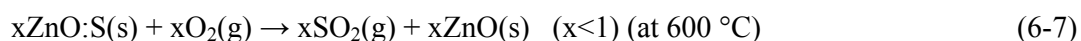
This strong DLE peak, without any peaks in the ultraviolet region for the S-doped ZnO nanobelts, and the blue-shift of the UV peak in the Sn-doped ZnO nanobelts provide strong evidence for successful S- and Sn-doping in ZnO nanobelts. Figures 6.4 (b) and (c) show the effect of thermal annealing at 600 °C for 1 h on the PL results of S- and Sn-doped ZnO nanobelts, respectively. It can be seen that a UV peak appears at 383 nm after annealing the S-doped ZnO nanobelts (as shown in the inset in Fig. 6.4 (b)). Additionally, the intensity of green emission of the S-doped ZnO nanobelts is significantly increased after annealing and the both peaks of green emission show a red-shift, but the blue emission is not shown any shifts after annealing. During the annealing process, oxygen and sulfur can easily escape from the S-doped ZnO nanobelts. Therefore, the concentration of oxygen vacancies increases, and the deformation defects that were attributed to the substitution of oxygen with sulfur decrease. Consequently, the appearance of a UV peak and the increase in the green emission intensity in the S-doped ZnO nanobelts after annealing could be attributed to these two factors.

It is known that when ZnO is doped with sulfur, the excess carriers supplied by the impurities to the conduction band contribute to increase electrical conductivity of ZnO and thus leads to a blue-shift of the UV peak. But, in our case not only the UV peak is not blue shifted by S but also we observe a slightly red-shift as comparison with the undoped ZnO nanobelts. This different behavior of the UV peak could be attributed to high content of S in this case. According to the theory of semiconductors,  $E_g$  increases when the impurity is kept under Mott critical density (Mott, 1974), and an abrupt  $E_g$  decrease transition happens while more impurity is doped into the semiconductor. Thereby, heavy doping usually induces an evidently narrowing of  $E_g$ . Higher S concentration in our ZnO nanobelts than the others can support this effect.

Figure 6.4 (c) shows that the PL result of the Sn-doped ZnO nanobelts is also affected by annealing. It can be seen that, the intensity of the UV and DLE peaks

increases after annealing. Furthermore, after annealing, the UV peak of the Sn-doped ZnO nanobelts shows a clear blue-shift to 372 nm (as shown in the inset in Fig 6.4 (c)). The annealing may have an effect on the activation of Sn. The UV/DLE ratio for the Sn-doped ZnO nanobelts is about 1.8 after and 1.5 before annealing. Therefore, the crystallinity of the Sn-doped ZnO nanobelts is improved by thermal annealing. In addition, the PL spectra of both nanobelts show a red-shift in the DLE peak after annealing. These shifts could be attributed to changes in the oxygen vacancy centers after annealing. However, the red-shift of the DLE peak for the S-doped (505 nm→515 nm) sample is greater than that of the Sn-doped (508 nm→512 nm) ZnO nanobelts. In fact, this larger shift of the DLE peak shows that the S-doped ZnO nanobelts are more affected by annealing than the Sn-doped ZnO nanobelts.

Based on the XRD results, it was observed that the crystallinity of the S-doped ZnO nanobelts was weaker than that of the Sn-doped ZnO nanobelts. Therefore, it is logical that the annealing should have a greater effect on the S-doped sample, as compared to the Sn-doped ZnO nanobelts. The process of annealing in the S-doped ZnO nanobelts may be described by the following reaction:



Therefore, after annealing, the S content decreases, and then, the structure of the S-doped ZnO nanobelts is closer to the ZnO structure, resulting in a UV peak that appears after annealing. Finally, from the PL results obtained for both types of nanobelts, it is shown that an anionic dopant can be greatly affected by annealing in air than a cationic dopant. In fact, the process of annealing in air that has a high amount of oxygen can have greater effects on sulfur than tin, because sulfur, due to its electronic shell, can more easily react with the available oxygen in the air. In addition, undoped ZnO nanobelts have annealed with the same conditions. Positions of the both peaks of the

undoped ZnO nanobelts have not been shown any changes and only their intensities have been increased by annealing, as the UV/DLE ratio have also been increased.

### 6.3. The effects of annealing temperature on structural and optical properties of S-doped ZnO nanobelts

Due to more annealing effect on S-doped ZnO nanobelts, the effects of annealing temperature on structural and optical properties of S-doped ZnO nanobelts are also investigated with more details. Figure 6.5 shows an FESEM image and EDX spectrum of S-doped ZnO nanobelts after annealing at 600 °C.

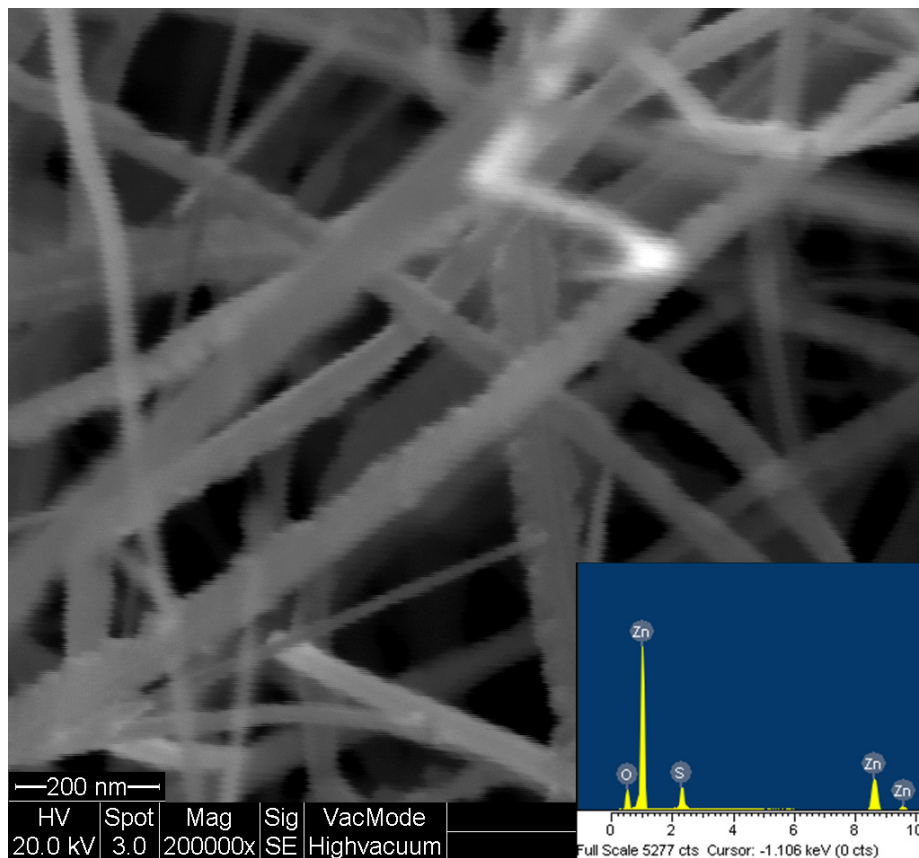


**Figure 6.5.** FESEM image and EDX spectrum of the S-doped ZnO nanobelts after annealing at 600 °C.

As shown in Fig. 6.5, the shape of nanobelts in comb side is changed slightly after annealing, and furthermore concentration of the S element is decreased to about 8% (atomic).

Figure 6.6 shows the XRD patterns of the as-grown and annealed samples at 400 and 600 °C for 1 h in an air atmosphere. All of the peaks intensities were increased by an increase in the annealing temperature. Also, the FWHM of the (101) peak decreased from 0.295° (as-grown sample) to 0.197° (annealed sample at 600 °C). Therefore, the crystalline quality and structure of the S-doped ZnO nanobelts were improved by the increase in the annealing temperature.

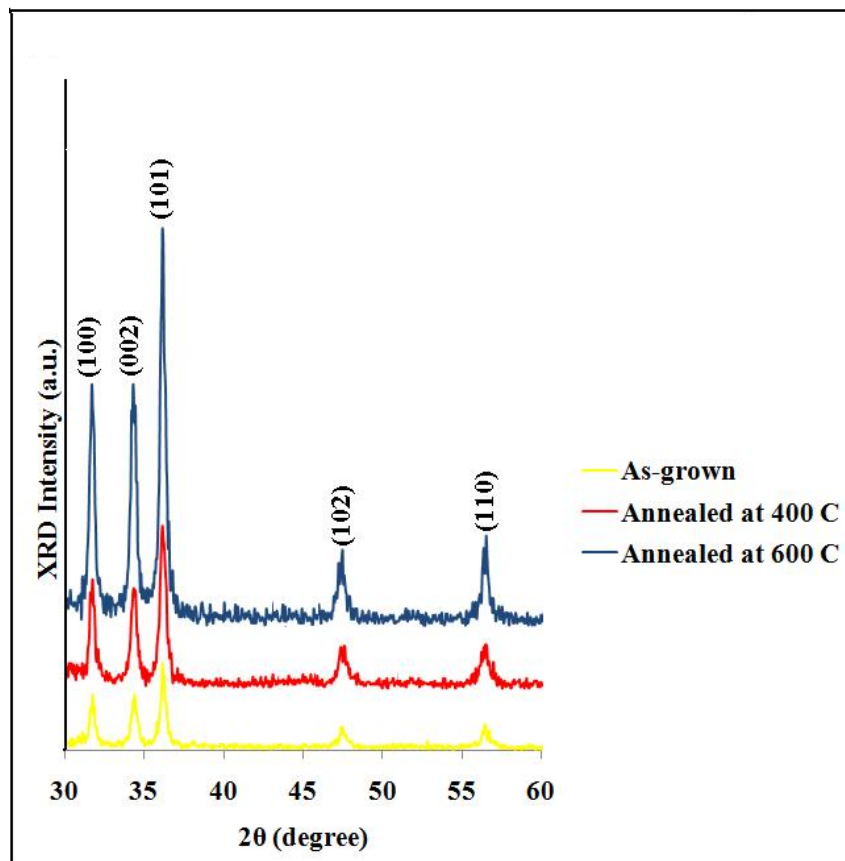


**Figure 6.6.** XRD patterns of the as-grown and annealed samples at 400 and 600 °C for 1 h in an air ambient. All peaks intensities increased with higher annealing temperature.

Figure 6.7 shows the effect of annealing at 400 and 600 °C for 1 h on the PL results of S-doped ZnO nanobelts. It can be seen that the UV peak intensity increases with the increase of the annealing temperature (UV peaks are shown in the inset in Fig. 6.7). In addition, the DLE/UV ratio is decreased from 34.8 to 29 by the increase of the

annealing temperature from 400 to 600 °C. This result has a significant agreement with the XRD result.

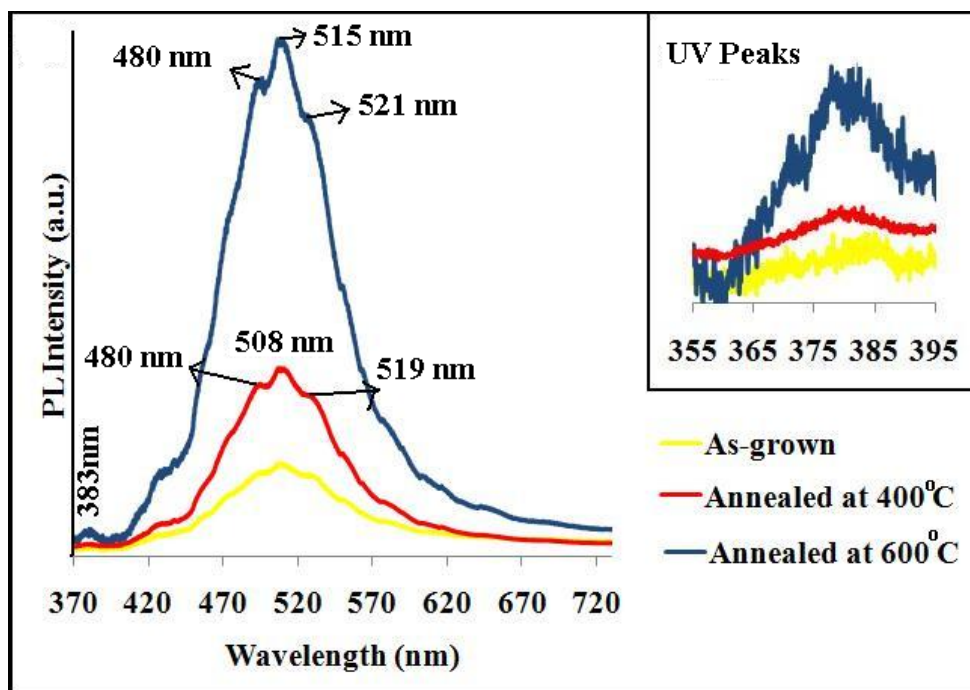


**Figure 6.7.** PL spectra of the S-doped ZnO nanobelts: as-grown and annealed at 400 and 600 °C for 1h in an air atmosphere. Intensity of the visible emission peaks increases with the increase of the annealing temperature. Also, the green emission peaks show a red-shift after annealing. The inset shows the appearance of a UV peak at 383 nm after annealing.

The Raman spectra for the S-doped and undoped ZnO nanobelts are presented in Fig. 6.8 (a). There is a significant difference between these two spectra that is similar to their PL. As shown in Fig. 6.8 (a), the Raman spectrum of undoped ZnO shows a sharp, strong, and dominant peak at  $437\text{ cm}^{-1}$  that corresponds to the  $E_2(\text{high})$  mode of the Raman active mode, while this mode for the S-doped ZnO nanobelts appears with weak intensity at  $428\text{ cm}^{-1}$ . Furthermore, a peak at  $331\text{ cm}^{-1}$ , assigned to the  $E_{2H} - E_{2L}$  mode indicates the presence of undoped ZnO nanobelts. A strong peak at  $565\text{ cm}^{-1}$  and a weak peak at  $579\text{ cm}^{-1}$  correspond to the  $E_1(\text{LO})$  for the S-doped and undoped ZnO nanobelts, respectively. Stronger  $E_1(\text{LO})$  and weaker  $E_2(\text{high})$  modes of the S-doped ZnO nanobelts in comparison to the  $E_1(\text{LO})$  and  $E_2(\text{high})$  modes of the undoped ZnO

nanobelts indicate a lower crystalline quality and higher oxygen vacancy of S-doped ZnO nanobelts than the undoped ZnO nanobelts.

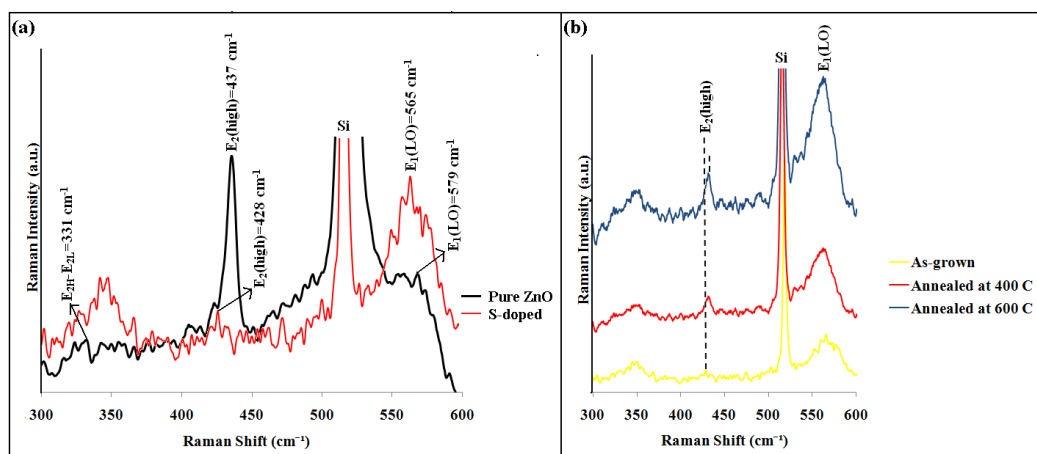


**Figure 6.8.** (a) Raman spectra of S-doped and undoped ZnO nanobelts. All Raman modes of the S-doped ZnO nanobelts show a red-shift relative to the Raman modes of the undoped ZnO nanobelts. (b) Raman spectra of the S-doped ZnO nanobelts: the nanobelts were as-grown and annealed at 400 and 600 °C for 1h in an air atmosphere. The intensity of the E<sub>2</sub>(high) and E<sub>1</sub>(LO) peaks increased with a higher annealing temperature. The E<sub>2</sub>(high) peak shows a blue-shift after annealing.

Moreover, the peaks of Raman active modes of the S-doped ZnO nanobelts are red-shifted relative to the undoped ZnO nanobelts. Usually, the Raman peak shifts for three reasons: phonon confinement effect (Lin *et al.*, 2006), higher volume density of the point defects (Xiu *et al.*, 2006), and lattice strain (Tiwari *et al.*, 2002). One of the most important sources for point defects is oxygen vacancies (Jiang *et al.*, 2007). Therefore, in our case the second reason may be dominant for the shift of the Raman peaks of the S-doped ZnO nanobelts, and the presence of a high intensity Raman active E<sub>1</sub>(LO) mode and red-shifts of the Raman peaks of the S-doped nanobelts are also strong evidence for successful S-doping in the ZnO nanobelts. Raman spectra of the as-grown and annealed samples (at 400 and 600 °C) of the S-doped ZnO nanobelts are shown in Fig. 6.8 (b). The intensity of the E<sub>2</sub>(high) and E<sub>1</sub>(LO) peaks increase with increased annealing temperature. In addition, the E<sub>2</sub>(high) mode peak is slightly blue-shifted by the increased annealing temperature. Therefore, the Raman results of the S-

doped ZnO nanobelts show that the crystalline quality is upgraded by an increase in the annealing temperature in addition to what the XRD and PL show.